Coarse-Grained Modeling of Proline Rich Protein 1 (PRP-1) in Bulk Solution and Adsorbed to a Negatively Charged Surface

Marie Skepö,*,† Per Linse,‡ and Thomas Arnebrant†

Health and Society, Malmö University, S-205 06 Malmö, Sweden, and Physical Chemistry 1, Lund University, Box 124, S-221 00 Lund, Sweden

Received: October 21, 2005; In Final Form: March 29, 2006

Structural properties of the acidic proline rich protein PRP-1 of salivary origin in bulk solution and adsorbed onto a negatively charged surface have been studied by Monte Carlo simulations. A simple model system with focus on electrostatic interactions and short-ranged attractions among the uncharged amino acids has been used. In addition to PRP-1, some mutants were considered to assess the role of the interactions in the systems. Contrary to polyelectrolytes, the protein has a compact structure in salt-free bulk solutions, whereas at high salt concentration the protein becomes more extended. The protein adsorbs to a negatively charged surface, although its net charge is negative. The adsorbed protein displays an extended structure, which becomes more compact upon addition of salt. Hence, the conformational response upon salt addition in the adsorbed state is the opposite as compared to that in bulk solution. The conformational behavior of PRP-1 in bulk solution and at charged surfaces as well as its propensity to adsorb to surfaces with the same net charge are rationalized by the block polyampholytic character of the protein. The presence of a triad of positively charged amino acids in the C-terminal was found to be important for the adsorption of the protein.

1. Introduction

The interaction between proteins and surfaces is essential for a number of applications such as biomaterials,[1] drug delivery,[2] biotechnical separation,[3] and food.[4,5] Knowledge of the fundamental interactions involved in protein adsorption is of great importance for understanding and controlling the interfacial behavior of proteins. During the past decades, a number of theoretical and numerical investigations have been performed on proteins interacting with surfaces.[6−18] For example, in colloidal-like models, the proteins are represented as particles and one can accurately predict adsorption kinetics and isotherms. Other approaches involve slab models, random sequential adsorption models, scaled particle theory, and fully molecular models. Common for these approaches is that they treat the electrostatic and van der Waals interactions between the colloidal particle and the surface and that they can capture dependencies on surface charge, protein size, and salt concentration. Moreover, with detailed atomistic representation, Ravichandran et al.[15] have found that a net positively charged protein could adsorb to a positively charged surface due to the nonuniformity of the charge distribution on the protein. Zhou et al.[16] predicted the orientations of an adsorbed antibody on a surface using a united residue model, where each amino acid was represented by a group with averaged electrostatic and van der Waals interactions. From many of these investigations, it has been concluded that protein adsorption depends strongly on ionic strength and pH; hence, electrostatic interactions are fundamental.

Salivary proteinaceous macromolecules, ranging from short peptides to high molecular weight mucins and differing in physicochemical properties, are essential in the ability of saliva to form oral films on solids, which is an important factor for the maintenance of oral health and surface integrity.[19] The acidic proline rich proteins (PRPs) are found only in saliva[20] and constitute 20−30% of salivary proteins.[21] Moreover, PRPs are associated with bacterial binding and lubrication.[22−24] As their name implies, PRPs have a high content of proline, which together with glycine and glutamine constitute 70−88% of the total amino acid content.[21,25]

The PRPs are encoded by the PRH1 and PRH2 gene loci and contain five common allelic variants: PRP-1, PRP-2, Db, PIF, and Pa, deviating by single amino acid substitutions (PRP-1, PRP-2, PIF, Pa) and a 21 amino acid internal repeat (Db).[26] Acidic PRPs are secreted as large and truncated PRPs due to post-translational proteolysis. PRPs 1−4 are related as follows: PRP-1 and PRP-2 both consist of 150 residues; the only difference is that the residue in position 50 is aspargine in PRP-1 and aspartate in PRP-2.[26] PRP-3 and PRP-4 correspond exactly to the first 106 residues of PRP-1 and PRP-2, respectively. The molecular weights are 16 and 11 kD for the long (PRP-1 and PRP-2) and short (PRP-3 and PRP-4) PRPs, and their isoelectric points are 4.7 and 4.1, respectively.[26,27]

The acidic PRP is highly asymmetrical with a 30-residue N-terminal phosphorylated domain (containing two serine phosphates) interacting with hydroxyapatite surfaces and calcium, a proline rich middle portion, and a C-terminal portion reported to mediate bacterial adhesion. The N-terminal end, in particular the first 30 residues, contains basically all negatively charged residues including two Ca-binding phosphoserines. The C-terminal end contains the positively charged amino acids and most of the proline, glutamine, and glycine amino acids.[21] Hence, PRPs are polyampholytes[28] of biological origin. Salivary PRPs bear a structural resemblance to caseins in milk, having a flexible structure and a highly segregated distribution of charged amino acids.[29,30]

PRPs are potent inhibitors of spontaneous precipitation of calcium phosphate salts from saliva and secondary crystal

* To whom correspondence should be addressed. E-mail: marie.skepo@hs.mah.se.
† Malmö University.
‡ Lund University.

10.1021/jp056033o CCC: $33.50
Published on Web 05/26/2006

growth[23,31] and adhere strongly to hydroxyapatite.[21,32,33] Furthermore, they are a major part of the acquired dental pellicle[34] and have been shown to selectively bind oral microorganisms such as *Streptococcus mutans* and *Actinomyces viscosus.*[22,23] Consequently, this group of proteins is considered to be of prime importance in the buildup process of dental plaque. They have therefore attracted substantial interest in studies of the mechanism behind this process[33,34] and in attempts to reduce its rate.[23,35] Experimental studies of salivary protein adsorption onto oral surfaces are reported in the litterature.[32,33,36−41] Film formation, adsorption isotherms, structural data, and interactions between surfaces (particles) covered by adsorbed films of salivary proteins[42,43] are of central importance to further understand subsequent bacterial binding and plaque development.

The present study is focused on the proline rich protein PRP-1 in bulk solution and adsorbed to a negatively charged surface, examined by Monte Carlo simulations using a simple model system. Conformational and other structural properties of PRP-1 have been determined under salt-free conditions and with monovalent salt. With no added salt, the protein forms a compact coil in bulk solution but becomes extended when being adsorbed to the surface. The positively charged C-terminal block constitutes the anchoring part, and the negatively charged N-terminal block stretches into the solution. As salt is added, the protein expands in bulk solution and contracts at the charged surface, eventually becoming more compact at the surface than in bulk solution. Our study has similarities with the investigation by Leermakers et al.,[9] who have used self-consistent-field theory to study the surface coverage and density profiles of adsorbed β-casein.

2. Model

A coarse-grained model has been adopted to examine bulk and interfacial properties of PRP-1. Each amino acid is represented by a single site, and since the PRP-1 does not possess any significant secondary structure due to its richness of proline, such a simple model should still be able to describe some coarse-grained features of PRP-1. All charges are explicitly described, and the solvent enters the model through its relative permittivity. The bulk simulations were performed using a cubic box, whereas a rectangular box with one negatively charged surface and one uncharged surface was used for the surface simulations.

2.1. Protein Solution. The flexible chainlike PRP-1 is represented by a freely jointed chain of hard spheres (beads) connected by harmonic bonds, where a bead is negatively charged, positively charged, or uncharged, and represents an amino acid. The nature of each bead was identified from the amino acid sequence for PRP-1, and it is assumed that an amino acid is protonated at pH < pK_a and deprotonated at pH > pK_a. Here, pH $\approx$ 7 was selected, corresponding to the pH in saliva. Under these conditions, PRP-1 has a net charge of $Z_p = -9$, arising from 17 negatively charged, 8 positively charged, and 125 uncharged amino acids.[26] The negative amino acids are located at position 2 (Asp), 4 (Asp), 5 (Glu), 6 (Asp), 8 (Ser), 10 (Glu), 11 (Asp), 18 (Asp), 21 (Asp), 22 (Ser), 23 (Glu), 27 (Asp), 28 (Glu), 29 (Glu), 46 (Asp), 51 (Asp), and 150 (Gln), and the positive ones are located at 30 (Arg), 74 (Lys), 91 (Arg), 103 (Arg), 106 (Arg), 108 (Arg), 129 (Lys), and 139 (Arg).

A bead radius of $R_{aa} = 2$ Å is used, which provides a realistic contact separation between charge entities and represents an accurate description of the Coulomb interaction. The radius is of course too small to represent the excluded volume of an amino acid, but this was regarded to be of less importance for the gross structure of PRP-1. Again for simplicity, we neglect that proline give rise to a less flexible chain as compared to other amino acids. The 25 counterions to the charged amino acids are treated explicitly.

2.2. Surface. The charged surface is modeled as a hard surface with negatively charged sites 2 Å beneath the surface. The sites are arranged in a two-dimensional quadratic lattice with the spacing $d_s = 6.9$ Å, and each site carries the charge $Z_s = -1$, resulting in a surface charge density similar to mica, $\sigma = 0.021\ e/\text{Å}^2$, with e denoting the elementary charge. The counterions to the surface are included explicitly as well.

2.3. Potential Energy. All interactions are assumed to be pairwise additive. The total potential energy of the system U_{tot} is given as a sum of the four contributions according to

$$U_{tot} = U_{hs} + U_{el} + U_{short} + U_{bond} \tag{1}$$

The hard-sphere potential U_{hs} is given by

$$U_{hs} = \sum_{i<j} u_{ij}^{hs}(r_{ij}) + \sum_i u^{surf}(z_i) \tag{2}$$

with the summation extending over amino acids, cations, and anions, where u_{ij}^{hs} represents the hard-sphere potential between two beads according to

$$u_{ij}^{hs}(r_{ij}) = \begin{cases} 0, & r_{ij} \geq R_i + R_j \\ \infty, & r_{ij} < R_i + R_j \end{cases} \tag{3}$$

and u^{surf} the hard-sphere−hard-surface potential given by

$$u^{surf}(z_i) = \begin{cases} 0, & 0 \leq z_i \leq L_z \\ \infty, & z_i < 0 \text{ or } z_i > L_z \end{cases} \tag{4}$$

The electrostatic potential energy U_{el} is given by

$$U_{el} = \sum_{i<j} u_{ij}^{el}(r_{ij}) = \sum_{i<j} \frac{Z_i Z_j e^2}{4\pi\epsilon_0\epsilon_r} \frac{1}{r_{ij}} \tag{5}$$

where the summations extend over all of the particles in the system (amino acids, cations, anions, and surface charges). In eqs 1−4, Z_i denotes the charge of particle i, R_i the radius of particle i, ϵ_0 the permittivity of vacuum, ϵ_r the relative permittivity of water, $r_{ij} \equiv |\mathbf{r}_i - \mathbf{r}_j|$ the distance between the centers of particles i and j, with $\mathbf{r}_i$ representing the position of particle i, and z_i the z-coordinate of particle i.

The nonelectrostatic attractive potential U_{short}, representing the hydrophobic interaction between the uncharged amino acids, is given by

$$U_{short} = -\sum_{i<j} \frac{\epsilon}{r_{ij}^6} \tag{6}$$

with ϵ being the parameter determining the strength of the nonelectrostatic interaction. This interaction is of complex nature, and since Kauzmann's review,[44] it has been widely appreciated that the hydrophobic interaction is of importance in protein folding. Several attempts have been made to quantify the degree of hydrophobicity of each amino acid. Values of the interaction parameter ϵ have been determined by using Eisenberg's[45] hydrophobicity scale, which is based on the free energies of transferring amino acid side chains from water to ethanol. Employing this scale, isoleucine (Ile) becomes the most hydrophobic amino acid in PRP-1, with $\epsilon \approx 1.23kT$, and glycine (Gly) the least hydrophobic one with $\epsilon \approx 0.07kT$. For simplicity, all of the uncharged amino acids are here assigned the same

TABLE 1: General Data of the Model

box length (surface system)	$L_x = L_y = 207$ Å, $L_z = 400$ Å
box length (bulk system)	$L_x = L_y = L_z = 276$ Å
amino acid radius	$R_{aa} = 2$ Å
amino acid charge	$Z_{aa} = -1, 0, +1$
small ion radius	$R_{ion} = 2$ Å
small ion charge	$Z_{ion} = -1, +1$
short-range attractive parameter	$\epsilon = 0.6kT$
surface charge spacing	$d_s = 6.9$ Å
surface charge density	$\sigma = 0.021$ e/Å^2
temperature	$T = 298$ K
relative permittivity	$\epsilon_r = 78.4$
1:1 salt concentration	$c_{salt} = 0, 20, 50, 80, 100$ mM

hydrophobicity. The value $\epsilon = 0.6kT$, obtained as the arithmetic average over the 125 uncharged amino acids, is used.

The remaining term in eq 1, U_{bond}, is the bond potential energy, which applies only to the protein. It is given by

$$U_{bond} = \sum_{i=1}^{N_{bead}-1} \frac{k_{bond}}{2}(r_{i,i+1} - r_0)^2 \qquad (7)$$

where $r_{i,i+1}$ denotes the distance between two connected beads with the equilibrium separation $r_0 = 5$ Å and force constant $k_{bond} = 0.4$ N/m and where $N_{bead} = 150$ is the number of beads representing the protein.

2.4. Systems. Properties of the PRP-1 model in bulk solution and in solution being in contact with a negatively charged surface have been determined. The conditions with monovalent protein and surface counterions but no additional salt will be referred to as salt-free conditions. The influence of salt is examined by employing salt concentrations up to $c_{salt} = 100$ mM 1:1 salt. In addition, one natural occurring and three artificial site-specific amino acid substitutions have been considered. They comprise the substitution of (I) Asn 50 by a negatively charged amino acid (corresponding to PRP-2, see Introduction), (II) Lys 129 by an uncharged amino acid, (III) Arg 106 by an uncharged amino acid, and (IV) a double-substitution where the negatively charged Arg 106 is replaced by an uncharged amino acid and the uncharged amino acid at position 134 is replaced by a positively charged amino acid. In the first three cases, the net charge of the protein is changed from -9 to -10, and in the fourth case, it is unchanged.

The bulk simulations were performed using a cubic box with a box length of 276 Å, and the surface simulations, using a rectangular box with box lengths $L_x = L_y = 207$ Å and $L_z = 400$ Å with one negatively charged surface at $L_z = 0$ and an uncharged surface at $L_z = 400$. At the highest salt concentration, the surface system comprises ~4000 particles. Throughout, $T = 298$ K and $\epsilon_r = 78.4$, thus representing water at ambient temperature. The main parameters of the surface systems are compiled in Table 1.

3. Method

3.1. Simulation Aspects. The equilibrium properties of the model systems were obtained by Metropolis Monte Carlo (MC) simulations[46,47] in the canonical ensemble, that is, constant number of particles, volume, and temperature. In the bulk simulations, periodical boundary conditions were applied in all three directions, whereas, in the surface simulations, periodical boundary conditions were applied in the *x*- and *y*-directions. Moreover, in the bulk simulations, the long-ranged Coulomb interactions were handled by using the Ewald summation technique,[46] while, in the surface simulations, all interactions were truncated using the minimum image convention. The examination of the configurational space was facilitated by using four different types of displacements of the protein: (i) translational displacement of a single bead, (ii) pivot rotation of a part of the protein chain, (iii) translation of the entire protein chain, and (iv) slithering move using a biased sampling technique. The small ions were only subjected to translational displacements.

The initial configurations were generated by placing the chain randomly in the box. The equilibrium phase of the simulations was performed using at least 2×10^5 passes (trial moves per particle), and the production runs involved at least 8×10^5 passes at $c_{salt} = 0-20$ mM and 1.6×10^6 passes at $c_{salt} = 50-100$ mM. During the production run, the root-mean-square (rms) displacement of the adsorbed protein was approximately 1200 Å at the different salt concentrations compared to the surface length 207 Å.

Throughout, the salt concentrations will be reported as being averaged over the simulated box. The bulk concentration of the system is represented by the salt concentration far away from the surface. Due to the slight inhomogeneous distribution of the salt species, these two concentrations differ somewhat. Since the differences are below 10% and of no consequence for our qualitative discussion on the effect of salt, we will for simplicity neglect this discrepancy.

The reported uncertainties of simulated quantities are one standard deviation of the mean as estimated by dividing the simulations into 10 sub-batches. Selected uncertainty bars are given in some of the figures. The simulations were performed by using the integrated Monte Carlo/molecular dynamics/Brownian dynamics simulation package Molsim.[48]

3.2. Analysis. The structural properties of the protein in bulk and adsorbed onto the charged surfaces have been characterized by several different quantities.

The extension of the protein has been quantified by the rms end-to-end distance, $\langle R_{ee}^2\rangle^{1/2} \equiv \langle|\mathbf{r}_1 - \mathbf{r}_{N_{bead}}|^2\rangle^{1/2}$, and the rms radius of gyration $\langle R_G^2\rangle^{1/2} \equiv \langle N_{bead}^{-1} \sum_{i=1}^{N_{bead}} (\mathbf{r}_i - \mathbf{r}_{com})^2\rangle^{1/2}$, with $\langle ...\rangle$ denoting an ensemble average and $\mathbf{r}_{com}$ the center of mass of the protein. Both quantities increase for a more extended protein configuration but depend differently on the shape. Consequently, the ratio $r \equiv \langle R_{ee}^2\rangle/\langle R_G^2\rangle$, also referred to as the shape ratio, provides information about the shape. In the rodlike limit, $r = 12$, whereas, for ideal (Gaussian) chains, $r = 6$.

A bead is considered to be adsorbed onto the surface if the distance between the bead and the surface does not exceed 10 Å from their contact separation. The probability that the bead with rank i_{aa} is adsorbed onto the surface will be denoted by $P_{ads}(i_{aa})$. The sum of $P_{ads}(i_{aa})$ over the N_{bead} beads represents the average number of adsorbed beads N_{ads}.

Another important property is the bead number density perpendicular to the surface $\rho(z)$. Finally, the functions $P(R_{G,z})$ and $P(z_{com})$ have been used, which represent the probability distribution of the radius of gyration projected on the *z*-direction and the probability distribution of the shortest distance between the surface and the center of mass of the protein.

4. Results

4.1. Protein in Bulk Solution. Panels a and b of Figure 1 provide snapshots of the protein under salt-free conditions and at 100 mM 1:1 salt. The snapshots indicate that (i) the protein is relatively compact under the salt-free conditions with a substantial degree of positive and negative amino acids being associated and (ii) the protein is extended at $c_{salt} = 100$ mM.

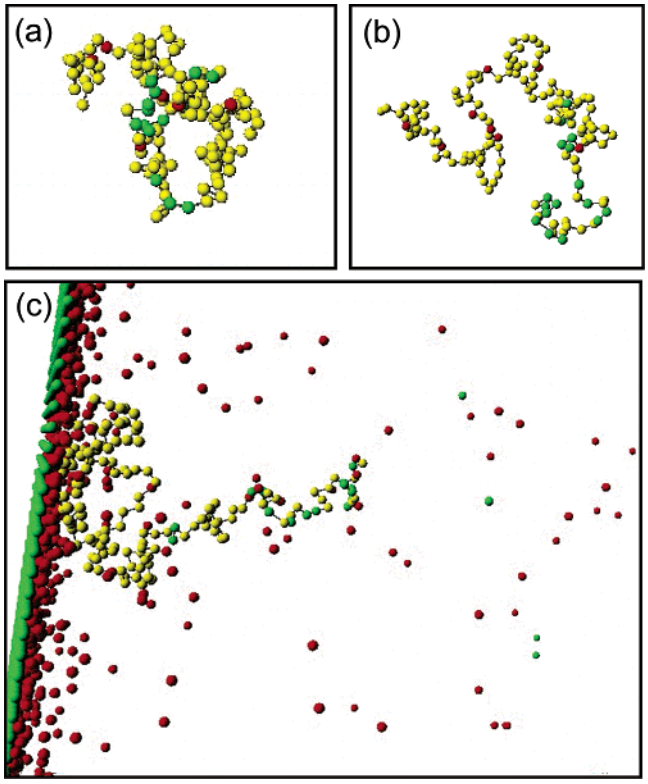

Figure 1. Snapshots of the PRP-1 model (a) in bulk under salt-free conditions, (b) in bulk at 100 mM 1:1 salt, and (c) adsorbed to a negatively charged surface under salt-free conditions. The simulated system contains a coil-like protein with 150 amino acids (connected dots), cations and anions (unconnected dots), and in part c one negatively charged surface. All of the particles are drawn to scale. Color code: positively charged amino acids and cations (red); negatively charged amino acids, anions, and surface charges (green); and uncharged amino acids (yellow). In parts a and b, the cations and anions are omitted for clearer visualization of the position of the charged amino acids.

TABLE 2: Root-Mean-Square (rms) Radius of Gyration ($\langle R_G^2\rangle^{1/2}$), rms End-to-End Distance ($\langle R_{ee}^2\rangle^{1/2}$), and Shape Factor ($r$) for PRP-1 in Bulk Solution at Different 1:1 Salt Concentrations[a]

c_{salt}/mM	$\langle R_G^2\rangle^{1/2}$/Å	$\langle R_{ee}^2\rangle^{1/2}$/Å	r
0	31	58	3.5
20	33	69	4.4
50	37	88	5.6
80	40	99	6.2
100	41	103	6.3

[a] The largest estimated uncertainties are $\sigma = 1$ and 2 Å for $\langle R_G^2\rangle^{1/2}$ and $\langle R_{ee}^2\rangle^{1/2}$, respectively.

This structural behavior upon salt addition is confirmed by conformational data at different salt concentrations compiled in Table 2. Under salt-free conditions, $\langle R_G^2\rangle^{1/2} = 31$ Å and $\langle R_{ee}^2\rangle^{1/2} = 58$ Å, which should be compared with a contour length of ~750 Å. From the increase of $\langle R_G^2\rangle^{1/2}$ and $\langle R_{ee}^2\rangle^{1/2}$, it is confirmed that the protein progressively becomes more extended at successive addition of the 1:1 salt. The salt effect levels off at $c_{salt} \approx 80$ mM, at which $\langle R_G^2\rangle^{1/2}$ has increased to ~40 Å and $\langle R_{ee}^2\rangle^{1/2}$ to ~100 Å. For comparison, a neutral 150 bead long chain where only the excluded volume repulsion among the beads is considered gives a $\langle R_G^2\rangle^{1/2}$ value of approximately 42 Å and a $\langle R_{ee}^2\rangle^{1/2}$ value of 107 Å. Also, the shape of the protein is affected. Under salt-free conditions, the shape factor becomes $r = 3.5$, implying a configuration much more spherical-like than a Gaussian coil, whereas, at $c_{salt} = 100$ mM, we have $r = 6.3$, demonstrating a protein somewhat more extended than a Gaussian coil.

TABLE 3: Root-Mean-Square (rms) Radius of Gyration $\langle R_G^2\rangle^{1/2}$, rms End-to-End Distance $\langle R_{ee}^2\rangle^{1/2}$, and Shape Factor ($r$) for PRP-1 Adsorbed to a Negatively Charged Surface at Different 1:1 Salt Concentrations[a]

c_{salt}/mM	$\langle R_G^2\rangle^{1/2}$/Å	$\langle R_{ee}^2\rangle^{1/2}$/Å	r
0	52	131	6.5
20	44	109	6.1
50	43	105	6.0
80	42	99	5.7
100	42	102	5.9

[a] The largest estimated uncertainties are $\sigma = 2$ and 5 Å for $\langle R_G^2\rangle^{1/2}$ and $\langle R_{ee}^2\rangle^{1/2}$, respectively.

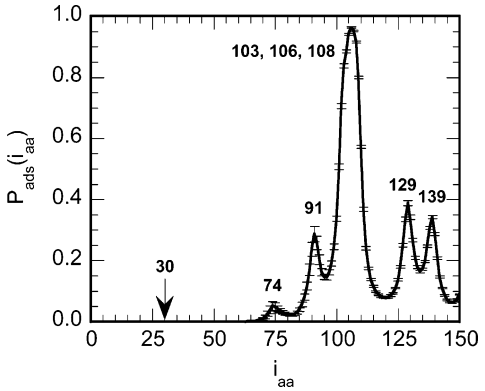

Figure 2. Amino acid adsorption probability $P_{ads}(i_{aa})$ versus the amino acid rank i_{aa} with uncertainty bars under salt-free conditions.

Hence, in the salt-free limit, we conclude that the intrachain electrostatic attraction between the negatively charged N-terminal block and the positively charged C-terminal block folds the protein to a relatively compact and spherical-like structure. On the contrary, at the highest salt concentration considered (at which the Debye screening length is 9 Å), the chain becomes more extended owing to the nearly completed screening of the attractive electrostatic interaction between the two oppositely charged blocks. The excluded volume repulsion between the beads makes $r > 6$. In both salt regimes, the contraction due to the hydrophobic attraction plays only a secondary role.

4.2. Protein Adsorbed to a Negatively Charged Surface. *4.2.1. Salt-Free Conditions.* During the equilibration phase, the protein became adsorbed, and the protein remained adsorbed during the entire production run. This is a strong indication that at equilibrium the protein is adsorbed to the surface.

A snapshot of the protein adsorbed to the surface under salt-free conditions is shown in Figure 1c. The protein appears to be relatively extended with the positively charged C-terminal block collapsed and attached on the surface, whereas the negatively charged N-terminal block forms a tail that stretches away from the surface. The snapshot also shows a strong accumulation of cations to the negatively charged surface.

Conformational data of the protein adsorbed to the surface at different salt concentrations are given in Table 3. Upon adsorption under salt-free conditions, we notice that $\langle R_G^2\rangle^{1/2}$ increases from 31 to 52 Å and $\langle R_{ee}^2\rangle^{1/2}$ increases from 58 to 131 Å, whereas the shape factor (r) increases from 3.5 to 6.5. Hence, under salt-free conditions, the protein undergoes a strong stretching when being adsorbed.

We will now examine which amino acids are anchored to the surface. The probability of each of the amino acids to be adsorbed to the surface $P_{ads}(i_{aa})$ is shown in Figure 2, and of special interest is the probabilities of the positively charged

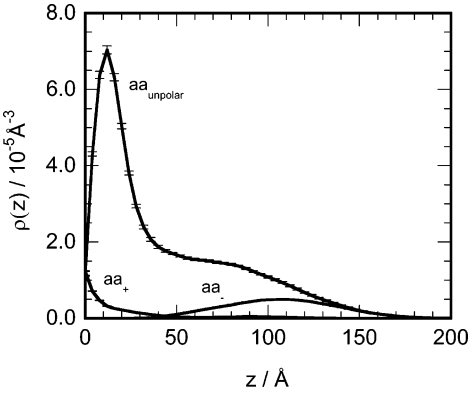

Figure 3. Amino acid number density distribution $\rho(z)$ in the z-direction for positively charged amino acids (aa_+), negatively charged amino acids (aa_-), and uncharged amino acids ($aa_{unpolar}$) with uncertainty bars under salt-free conditions. The position $z = 0$ corresponds to hard-sphere contact with the surface.

TABLE 4: Number of Amino Acids of PRP-1 within 10 and 20 Å from the Negatively Charged Surface at Different 1:1 Salt Concentrations

c_{salt}/mM	N_{ads} (10 Å)	N_{ads} (20 Å)
0	18.2	48
20	16.9	46
50	14.5	41
80	13.1	36.9
100	9.5	27.8

amino acids. As anticipated, the largest probabilities appear for amino acids in the positively charged C-terminal block, whereas the probability is zero for the first 70 amino acids of the N-terminal block. In more detail, a nearly unit adsorption probability is obtained for the region containing the three positively charged amino acids 103, 106, and 108. Moreover, significant adsorption probabilities appear for the positively charged amino acids 91, 129, and 139. The adsorption probability is below 0.1 for amino acid 74 and zero for amino acid 30. The average number of adsorbed amino acids within 10 Å from the surface is 18.2. Thus, (i) the three positively charged amino acids located close to each other in the primary sequence facilitate that part of the protein to become adsorbed, (ii) the positively charged amino acid within the negatively charged N-terminal block is not adsorbed, and (iii) the remaining positively charged amino acids display intermediate adsorption probabilities.

Figure 3 displays the number density $\rho(z)$ of the amino acids in the neighborhood of the surface, separated into positively charged, negatively charged, and uncharged amino acids. It is seen that the 8 positively charged and the 17 negatively charged amino acids form two separated layers. The former extends 40 Å from the surface, and the negatively charged amino acids are located between 50 and 170 Å away from the surface. The uncharged amino acids are present across the two layers and have a density maximum ~12 Å from the surface. Approximately half of the uncharged amino acids are within the layer of the positively charged amino acids. Thus, the number density distributions fully support the picture provided by Figure 1c that (i) the positively charged C-terminal block adsorbs at the surface and (ii) the negatively charged N-terminal block forms an extended tail stretching away from the surface.

4.2.2. Addition of 1:1 Salt. Of special interest is to analyze how the addition of monovalent salt affects the adsorption behavior. Four different salt concentrations, $c_{salt} = 20$, 50, 80, and 100 mM, have been investigated. For comparison, the monovalent salt concentration in saliva is ~85 mM and the physiological salt concentration in the body is ~150 mM.

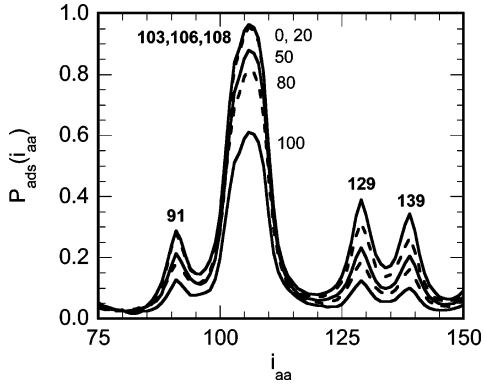

Figure 4. Amino acid adsorption probability $P_{ads}(i_{aa})$ versus the amino acid rank i_{aa} for the C-terminal block at 0, 20, 50, 80, and 100 mM 1:1 salt (alternating solid and dashed curves).

As for the salt-free conditions, the protein was adsorbed throughout the production simulations. However, Table 4 shows that the number of amino acids near the charged surface decreases as the salt concentration is increased. At $c_{salt} = 100$ mM, only half of the adsorbed amino acids remain.

The conformational data in Table 3 show that $\langle R_G^2 \rangle^{1/2}$ decreases from 52 to 42 Å, $\langle R_{ee}^2 \rangle^{1/2}$ decreases from 131 to 102 Å, and the shape factor r decreases from 6.5 to 5.9 as c_{salt} is increased from 0 to 100 mM. Thus, upon salt addition, the adsorbed protein contracts and becomes less extended. This response on the salt addition is the opposite of that which appeared for the protein in bulk solution. Noticeably, at $c_{salt} = 100$ mM, the protein is slightly more compact at the surface than in bulk solution.

Figure 4 shows $P_{ads}(i_{aa})$ at different salt concentrations. Generally, the probability of the amino acids in the C-terminal block to remain adsorbed is reduced at increasing c_{salt}. A comparison between the salt-free system and $c_{salt} = 20$ mM shows that the decrease starts with amino acids 120−150 in the end of the C-terminal block, with the adsorption probabilities of the positively charged amino acids 74, 91, 103, 106, and 108 being unaffected. When c_{salt} is raised to 50, 80, and 100 mM, the decrease of the adsorption is more pronounced and appears for the whole C-terminal block, but still none of the charged groups are completely released from the intimate neighborhood of the surface.

The distributions of the different types of amino acids perpendicular to the surface at different salt concentrations are shown in Figure 5. The changes for the positively charged amino acids are relatively small, but the number density near the surface is reduced at higher salt concentration (Figure 5a). The change of the distribution of the negatively charged amino acids is more prominent. There is a shift toward the surface at increasing salt concentration (Figure 5b). Finally, the density of the uncharged amino acids reduces within the first 20 Å and beyond 70 Å, whereas in between the density is increased (Figure 5c).

The dimension and the position of the adsorbed protein has been further quantified by analyzing the probability distributions of the radius of gyration projected on the z-axis $P(R_{G,z})$ and the location of the center of mass relative to the surface $P(z_{com})$ at different salt concentrations. Figure 6a shows that the most probable $R_{G,z}$ reduces from 40 Å in the salt-free system to 20 Å at $c_{salt} = 100$ mM, with half of the change occurring already at 20 mM. Noticeable are the wide distributions showing large fluctuations of the longitudinal extension. Figure 6b shows that

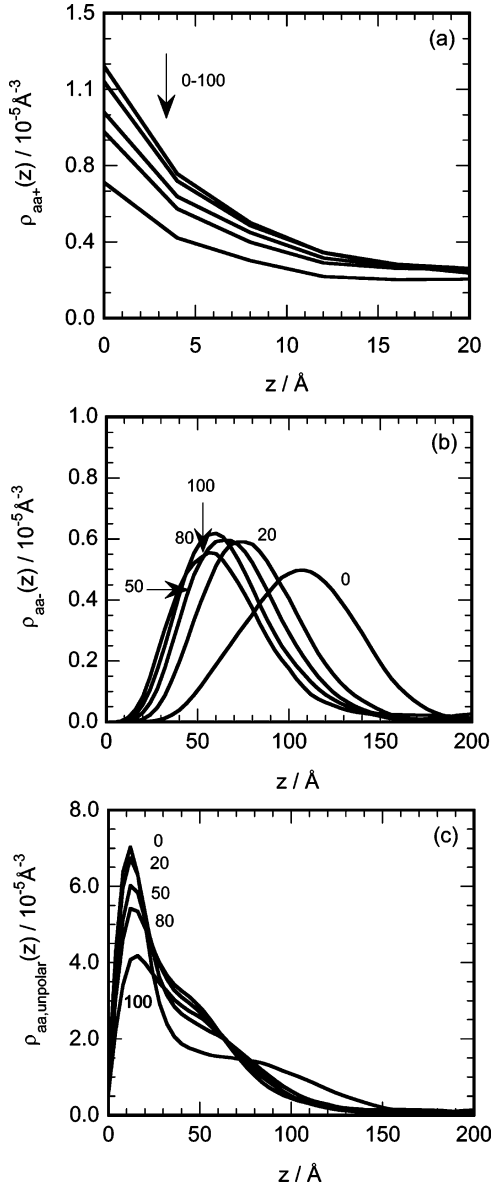

Figure 5. Amino acid number density distribution $\rho(z)$ in the z-direction for (a) positively charged amino acids (aa_+), (b) negatively charged amino acids (aa_-), and (c) uncharged amino acids ($aa_{unpolar}$) at 0, 20, 50, 80, and 100 mM 1:1 salt. The position $z = 0$ corresponds to hard-sphere contact with the surface.

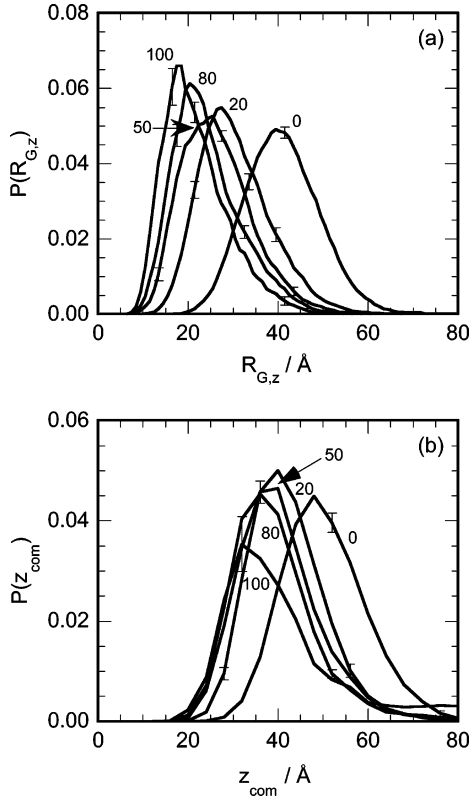

Figure 6. Probability distribution function of (a) the radius of gyration $P(R_{G,z})$ and (b) the center of mass $P(z_{com})$ of the protein at 0, 20, 50, 80, and 100 mM 1:1 salt. Selected uncertainty bars are given.

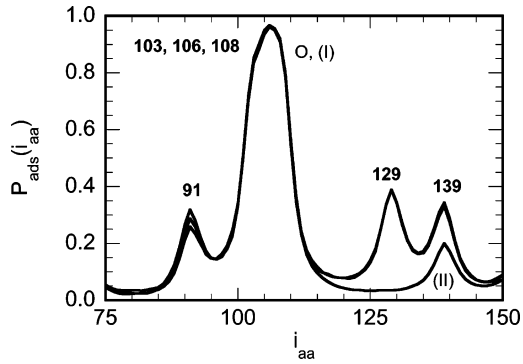

Figure 7. Amino acid adsorption probability $P_{ads}(i_{aa})$ versus the amino acid rank i_{aa} for PRP-1 (labeled "O") and two related proteins obtained by amino acid substitutions at positions 50 (substitution I) and 129 (substitution II) (see text) under salt-free conditions.

the most probable location of the center of mass is shifted from 50 to 35 Å from the surface at increasing salt concentration, again a significant response appearing already at 20 mM. Also, the position of the center of mass displays large fluctuations at all salt concentrations.

It is, hence, evident that upon salt addition the adsorbed protein becomes (i) weaker anchored at the surface and (ii) more contracted. The former issue is primarily due to the screening of electrostatic attraction between the C-terminal block and the surface, and the latter one is due to the screening of the electrostatic repulsion between the N-terminal block and the surface and within the N-terminal block.

4.2.3. Amino Acid Substitutions. Four substitutions have been made, all investigated under salt-free conditions. Substitution I, involving the replacement of the uncharged Asp 50 with a negatively charged amino acid, did not significantly change any conformational properties, adsorption probabilities of individual amino acids (Figure 7), or amino acid distributions normal to the surface. Thus, the increase of the absolute charge of the negatively charged N-terminal block, constituting the tail of the adsorbed protein, by one elementary unit does not affect the adsorption.

The replacement of the positively charged amino acid 129 by an uncharged one (substitution II) still led to an adsorbed protein. Although the protein is still as firmly anchored by the three positively charged amino acids 103, 106, and 108, Figure 7 shows that the loss of the positively charged amino acid at position 129 leads to significant weakening of the adsorption of the end of the C-terminal block. No major changes of conformational properties or the amino acid density distribution at the surface appeared.

On the contrary, the replacement of the positively charged amino acid Arg 106 by an uncharged one (substitution III) led to the situation that the protein did not adsorb at the surface at all. The density distribution functions $\rho(z)$ showed that the protein was far from the surface and the $P_{ads}(i_{aa})$ values were

identical to zero (data not shown). In addition, the conformation data, $\langle R_G^2\rangle^{1/2} = 41$ Å, $\langle R_{ee}^2\rangle^{1/2} = 100$ Å, and $r = 5.7$, show that mutant III is more extended than the native one in bulk at $c_{salt} = 0$. This is reasonable, since the electrostatic intraprotein attraction is diminished.

The double-substitution IV involves the replacement of the positively charged Arg 106 with an uncharged amino acid and the replacement of the uncharged amino acid at position 134 with a positively charged amino acid, implying no change of the protein net charge. Nevertheless, this substitution made the protein nonadsorbing, supporting the notion that the triad of positively charged amino acids at 103, 106, and 108 is important for the adsorption of the overall negatively charged PRP to the negatively charged surface.

5. Discussion

5.1. PRP-1 as a Diblock Polyampholyte. Polymers that carry both negative and positive charges are classified as polyampholytes (PAs). The distribution of the charges along the chain and the net charge of the PA are two important factors that strongly influence the solubility of PAs and the interaction between PAs with other charged macromolecules.

The electrostatic interaction has a dual role on the extension of a PA. The interaction among unlike charges generally leads to a contraction of the PA in solution, whereas the presence of a net charge acts in the opposite direction. Hence, at a sufficiently large net charge, the net effect of the electrostatic interaction gives rise to an extension of the chain (as for polyions), whereas, below that limit, it leads to a contraction of the chain. The former case is referred to as the polyelectrolyte (PE) regime and the latter as the PA regime.

The effect of salt is the opposite in the two regimes. In the PE regime, a chain contracts upon salt addition, since the repulsive force behind the chain extension is screened. In the PA regime, the corresponding salt addition screens the electrostatic attraction between the blocks, leading to a chain expansion.

The location of the transition between the PE and PA regimes depends on the charge distribution. With a random charge distribution, the transition appears already at a small net charge, whereas, with a blockier charge distribution, this limit is shifted to a larger net charge.

At pH 7, we have already concluded that PRP-1 has a net charge of -9 with the N-terminal block carrying a net negative charge and the C-terminal block a net positive charge. The charge separation of the protein is strong; only one negative charge is located in the C-terminal block and one positive charge in the N-terminal block. Hence, PRP-1 is a naturally occurring diblock PA with strong charge segregation.

5.2. Bulk Solution. (i) In a salt-free solution, PRP-1 displayed a compact conformation, and (ii) upon salt addition, PRP-1 became more expanded. These two properties are hallmarks for the PA regime. Hence, we conclude that in bulk the electrostatic interblock attraction between the N- and C-terminal blocks is of major importance and folds the protein to a compact structure (Figure 1a). The effects of the interblock attraction obviously dominate over the intrablock repulsions. At high salt concentration, this attraction is screened and in combination with the excluded volume repulsion between the beads gives PRP-1 an extended structure (Figure 1b).

5.3. Adsorbed State. *5.3.1. General.* Under salt-free conditions, the net negatively charged PRP-1 displayed a strong adsorption to a negatively charged surface. The adsorbed state was characterized by a strong spatial separation of the N- and C-terminal blocks (Figure 1c). Hence, the conformation of PRP-1 changes drastically upon adsorption. The spatial charge separation is driven by the electrostatic field generated by the charged surface and its counterions. The positively charged C-terminal block was located close to the surface, where the field is strongly negative, and the N-terminal block further away, where the field is less negative. Despite the fact that the C-terminal block has a smaller absolute charge as compared to the N-terminal one, the net electrostatic interaction is sufficient for PRP-1 to adsorb. This picture is also consistent with the observed chain conformations at salt addition. At low salt concentration (20 mM), the salt primarily screens the repulsion of the N-terminal block from the surface (Figure 5b), leading to a more compact protein (Table 3) without strong influence on the adsorption of the C-terminal block (Figure 5a and Table 4). However, at higher salt concentration, the screening reduces the attraction of the C-terminal block to the surface (Figure 5a and Table 4), leading to a weaker adsorbed protein. Hence, at not too low salt concentration, PRP-1 displays the same behavior as a polyion — the adsorption weakens upon salt addition. For both polyions and PAs, the adsorption to a charged surface is driven by attractive electrostatic interactions, which diminish as salt is added.

5.3.2. Comparison with Experiments. We will now discus more salient features of the PRP-1 adsorption and make a comparison with experimental findings.

Under salt-free conditions, PRP-1 was adsorbed through its positively charged C-terminal block. The probable mechanism of the desorption of PRP-1 at increasing salt concentration is that the tail of the C-terminal block is first detached, thereafter, the amino acids at positions 91, 129, and 139 leave the surface, and finally, the last attachment point, the triad 103, 106, and 108, is detached. The most pronounced changes appeared in the range up to 20 mM. At physiological conditions, the salt dependence was weak.

Our results showed that the triad of charges at positions 103, 106, and 108 is crucial for the adsorption. The removal of the charge at position 106 was sufficient to make the protein nonadsorbing. PRP-1 can be cleaved by post-translational proteolysis between residues 106−107, forming the truncated form PRP-3. Experimentally, it was found that in aqueous 1 mM NaCl solution PRP-3 adsorbs much weaker than PRP-1 to negatively charged silica surfaces,[40] consistent with our findings.

A stretching of the molecule was observed upon adsorption under salt-free conditions. It is well-known that conformational changes take place for proteins upon adsorption.[49] For PRP-1 specifically, conformational changes of the molecule upon adsorption have been suggested to explain bacterial binding when adsorbed to hydroxyapatite but not in bulk solution.[50] Due to the charge sign and density of mica, conformational changes are, however, not expected to correlate with those at hydroxyapatite.

Surface force measurements on PRP-1 adsorbed on mica have been reported.[42] In 1 mM NaCl aqueous solution, a weakly adsorbed layer was formed, which was squeezed out when the surface separation became ∼80 Å. This surface separation is consistent with our finding of a dense protein layer of ∼40 Å (Figure 3).

Hence, the results of the present simulation study are supported by a number of different experimental observations. Thus, it appears that the present coarse-grained model with focus on electrostatic interaction and chain connectivity is sufficient to capture some essential aspects of the adsorption of PRP-1 onto charged surfaces.

6. Conclusions

There is substantial interest to relate results of bacterial binding assays[51,52] or measurements of intraoral lubrication[24,53] to the structure in adsorbed layers of salivary proteins. In the present study, we have initiated such possibilities by establishing a coarse-grained model of the proline rich protein PRP-1 solved by Monte Carlo simulations. This model is used to evaluate structural changes in bulk solution and in the adsorbed state upon changes in electrolyte concentration.

Our observations could fully be understood by considering PRP-1 under physiological conditions as a diblock polyampholyte. Despite its net charge −9, influences of the diblock structure were more important. For example, in bulk, PRP-1 is compact under salt-free conditions and expands upon addition of salt. Moreover, PRP-1 adsorbs to a negatively charged surface, and upon salt addition, the protein becomes less extended. We have shown that the triad of positive charges in the C-terminal bock is crucial for the adsorption.

In this contribution, we have focused on dilute protein conditions and therefore the results are limited to the structural aspects of a single protein. We also selected a surface with a charge density corresponding to mica to facilitate comparisons with experimental in vitro data. As to in vivo conditions, where PRP-1 is anticipated to bind to hydroxyapatite, the orientation of adsorbed PRP-1 is expected to be reversed. In forthcoming studies, finite protein concentration, addition of divalent salt, and adsorption at net neutral or positively charged surfaces will be addressed.

Acknowledgment. The work was supported by grants from Malmö University, the Knowledge foundation (KK-stiftelsen), Biofilms-research center for biointerfaces, and computing resources by LUNARC.

References and Notes

(1) Mrksich, M.; Whitesides, G. M. *Annu. Rev. Biophys. Biomol. Struct.* **1996**, *25*, 55−78.
(2) Arnebrant, T., Ed. Protein Adsorption in the Oral Environment. In *Biopolymers at Interfaces*; Marcel Dekker: New York, 2003.
(3) Rabel, S. R.; Stobaugh, J. F. *Pharm. Res.* **1993**, *10*, 171−186.
(4) Dickinson, E. *Food Hydrocolloids* **1986**, *1*, 3−23.
(5) Tolstoguzov, V. B. *Food Hydrocolloids* **1991**, *4*, 429−468.
(6) Adamczyk, Z.; Zembala, M.; Siwek, B.; Warszynski, P. *J. Colloid Interface Sci.* **1990**, *140*, 123−137.
(7) Yoon, B. J.; Lenhoff, A. M. *J. Phys. Chem.* **1992**, *96*, 3130−3134.
(8) Roth, C. M.; Lenhoff, A. M. *Langmuir* **1995**, *11*, 3500−3509.
(9) Leermakers, F. A. M.; Aktinson, P. J.; Dickinson, E.; Horne, D. *J. Colloid Interface Sci*. **1996**, *178*, 681−693.
(10) Oberholzer, M. R.; Wagner, N. J.; Lenhoff, A. M. *J. Chem. Phys.* **1997**, *107*, 9157−9167.
(11) Zhdanov, V. P.; Kasemo, B. *J. Chem. Phys.* **1998**, *109*, 6497−6501.
(12) Zhdanov, V. P.; Kasemo, B. *Surf. Rev. Lett.* **1998**, *5*, 615−634.
(13) Wijmans, C. M.; Dickinson, E. *Langmuir* **1999**, *15*, 8344−8348.
(14) Wijmans, C. M.; Dickinson, E. *Phys. Chem. Chem. Phys.* **1999**, *1*, 2141−2147.
(15) Ravichandran, S.; Madura, J. D.; Talbot, J. *J. Phys. Chem. B* **2001**, *105*, 3610−3613.
(16) Zhou, J.; Chen, S.; Jiang, S. *Langmuir* **2003**, *19*, 3472−3578.
(17) Carlsson, F.; Hyltner, E.; Arnebrant, T.; Malmsten, M.; Linse, P. *J. Phys. Chem. B* **2004**, *108*, 9871−9881.
(18) Gray, J. J. *Curr. Opin. Struct. Biol.* **2004**, *14*, 110−115.
(19) Mandel, I. D. *J. Dent. Res.* **1986**, *66*, 623−627.
(20) Schenkels, L. C. P. M.; Veerman, E. C. I.; Nieuw Amerongen, A. V. N. *Crit. Rev. Oral Biol. Med.* **1995**, *6*, 161−175.
(21) Hay, D. I. In *CRC Handbook of Experimental Aspects of Oral Biochemistry*; Lazzari E. P., Ed.; CRC Press: Boca Raton, FL, 1983; Vol. 22, pp 9−355.
(22) Gibbons, R. J.; Hay, D. I. *Infect. Immun.* **1988**, *56*, 439−445.
(23) Gibbons, R., Hay, D. I., Eds. *Adsorbed Salivary Proline-Rich Proteins as Bacterial Receptors on Apatitic* Surfaces; Springer-Verlag: New York, 1989.
(24) Hahn-Berg, I. C.; Lindh, L.; Arnebrant, T. *Biofouling* **2004**, *20*, 65−70.
(25) Bennick, A. *J. Dent. Res.* **1987**, *66*, 457−461.
(26) Hay, D. I.; Ahern, J. M.; Schluckebier, S. K.; Schlesinger, D. H. *J. Dent. Res.* **1994**, *73*, 1717−1726.
(27) Johnsson, M.; Levine, M. J.; Nancollas, G. H. *Crit. Rev. Oral Biol. Med.* **1993**, *4*, 371−378.
(28) Dobrynin, A. V.; Colby, R. H.; Rubinstein, M. *J. Polym. Sci.* **2004**, *42*, 3513−3538.
(29) Eigel, W. N.; Butler, J. E.; Ernstrom, C. A.; Farrell, H., M.; Harwalkar, V. R.; Jenness, R.; McL Whitney, R. *J. Dairy Sci.* **1984**, *67*, 1599−1631.
(30) Holt, C.; Sawyer, L. *Protein Eng.* **1988**, *2*, 251−259.
(31) Moreno, E. C.; Zahradnik, R. T. *J. Dent. Res.* **1979**, *58*, 896−903.
(32) Hay, D. I. *Arch. Oral Biol.* **1967**, *12*, 937−946.
(33) Moreno, E. C.; Kresak, M.; Hay, D. I. *J. Biol. Chem.* **1982**, *257*, 2981−2989.
(34) Bennick, A.; Chau, G.; Goodlin, R.; Abrams, S.; Tustian, D.; Madapallimattam, G. *Arch. Oral Biol.* **1983**, *28*, 19−27.
(35) Perinpanayagam, H. E. R.; van Wuyckhuyse, B. C.; Ji, Z. S.; Tabak, L. A. *J. Dent. Res.* **1995**, *74*, 345−350.
(36) Baier, R. E.; Glantz, P. O. *Acta Odontol. Scand.* **1978**, *36*, 289−301.
(37) Vassilakos, N.; Arnebrant, T.; Glantz, P.-O. *Scand. J. Dent. Res.* **1992**, *100*, 346−353.
(38) Vassilakos, N.; Arnebrant, T.; Glantz, P.-O. *Scand. J. Dent. Res.* **1993**, *101*, 133−137.
(39) Lindh, L.; Arnebrant, T.; Isberg, P.-E.; Glantz, P.-O. *Biofouling* **1999**, *14*, 189−196.
(40) Lindh, L. *Swed. Dent. J.* **2002**, Suppl. 152, 1−56.
(41) Lindh, L.; Glantz, P.-O.; Isberg, P.-E.; Arnebrant, T. *Biofouling* **2001**, *17*, 227−239.
(42) Nylander, T.; Arnebrant, T.; Baier, R. E.; Glantz, P.-O. *Prog. Colloid Polym. Sci.* **1998**, *108*, 34−39.
(43) Nylander, T.; Arnebrant, T.; Glantz, P.-O. *Colloids Surf., A* **1997**, *129−130*, 339−344.
(44) Kauzmann, W. *Adv. Protein. Chem.* **1959**, *14*, 1.
(45) Eisenberg, D.; Weiss, R. M.; Terwilliger, T. C.; Wilcox, W. *Faraday Symp. Chem. Soc.* **1982**, *17*, 109−120.
(46) Allen, M. P.; Tildesley, D. J. *Computer Simulations of Liquids*; Oxford: New York, 1987.
(47) Frenkel, D.; Smit, B. *Understanding Molecular Simulation*; Academic Press: San Diego, CA, 1996.
(48) Linse, P. *Molsim*, version 3.0 ed.; Lund University: Sweden, 1999.
(49) Guldbrand, L.; Nilsson, L.; Nordenskiöld, L. *J. Chem. Phys.* **1986**, *85*, 6686−6698.
(50) Gibbons, R. J.; Hay, D. I.; Childs, W. C., III; Davis, G. *Arch. Oral Biol.* **1990**, Suppl. 35, 107S−114S.
(51) Strömberg, N.; Ahlfors, S.; Borén, T.; Bratt, P.; Hallberg, K. *Adv. Exp. Med. Biol.* **1996**, *408*, 9−24.
(52) Strömberg, N.; Borén, T.; Carlén, A.; Olson, J. *Infect. Immun.* **1992**, *60*, 3278−3286.
(53) Hahn Berg, I. C.; Rutland, M. W.; T, A. *Biofouling* **2003**, *19*, 365−369.